JARS Journal of Applied Remote Sensing

RESEARCH PAPER

Synthetic aperture radar image change detection based on image difference denoising and fuzzy local information C-means clustering

Yuqing Wu, Qing Xu,* Xinming Zhu, Tianming Zhao, Bowei Wen, and Jingzhen Ma
Information Engineering University, The Institute of Geospatial Information, Zhengzhou, China

ABSTRACT. Deep neural network-based synthetic aperture radar (SAR) image change detection algorithms are affected by coherent speckle noise in the original image. Existing denoising methods have predominantly focused on generating binary images based on the pre-classification of original pixels, which is insufficient in removing interfering noise. Herein, to further reduce the noise points generated in the clustering algorithm, we combined the characteristics of the fuzzy clustering algorithm, demonstrating the obvious advantages of the proposed fast and flexible denoising convolutional neural network (FFDNet-F) method. An FFDNet was used to reduce noise interference in real SAR images and improve the detection accuracy and robustness of the method. Difference operators were then drawn from the weak noise images, and fuzzy local information C-means clustering was applied for analysis to generate the change detection results. The experimental results from two real datasets and the comparative analysis with other network models demonstrated the effectiveness of this method. Simultaneously, Gaofen-3 satellite images were used to verify and analyze surface flood disasters in Zhengzhou, China. The findings of this study demonstrate a significant improvement in detection accuracy using the proposed method compared with that of other algorithms.

Keywords: change detection; FFDNet; fuzzy clustering; image noise reduction; SAR image; noise interference

Paper 230522G received Oct. 5, 2023; revised Feb. 22, 2024; accepted Feb. 26, 2024; published Apr. 2, 2024.

1 Introduction

With the emerging development of earth observation systems, synthetic aperture radar (SAR) has received extensive attention because it is minimally restricted by natural conditions.[1] SAR image change detection is an important means of SAR image use.[2–4] Compared with the threshold method, the clustering algorithm does not need to model and analyze the speckle noise and is, therefore, more widely used. Currently, deep learning is also being used by many researchers. Although many new methods have been proposed to address speckle noise suppression in SAR images, it still remains a challenge.

To suppress speckle noise, Yousif and Ban[5] used principal component analysis to reduce the dimension of feature vectors and nonlocal means algorithms to reduce noise and detect changes in SAR images. In the basic process of change detection, improving the single difference map has become the research subject for many scholars. Li et al.[6] divided the image into low frequency and high frequency components to fuse different modes Liu et al.[7] used the mean ratio and difference operator for a simple linear combination and proposed a mean ratio-subtraction difference

*Address all correspondence to Qing Xu, xq2021ch@126.com

plot. Fusion difference maps improve the disadvantages of single difference maps; however, some limitations in utilizing image information remain. Gao et al.[8] utilized frequency domain analysis to improve the quality of difference maps, effectively reducing noise interference and enhancing change detection accuracy. Afterwards, the research team applied the FCM clustering algorithm for change detection. FCM is a clustering algorithm based on fuzzy theory that groups sample data into distinct categories according to their similarity. By using the FCM algorithm, pixels with similar features and attributes can be classified into cohesive categories, automatically adapting to complex backgrounds and noise conditions within the dataset proficiently.

Many researchers have conducted in-depth studies on change detection using traditional clustering and the corresponding improved clustering algorithms.[9] Three-channel fusion differential images, classified using k-means, have been established in the literature, and an unsupervised clustering SAR image change detection algorithm, which was found to overcome the problem of statistical model selection, has been proposed.[10] Ahmed et al.[11] proposed an improvement of the FCM algorithm, which introduces spatial neighborhood information into the fuzzy C-means (FCM) objective function. Gao et al.[12] applied the FCM algorithm for the pre-classification of pixels and combined it with an extreme learning machine algorithm. Few studies have applied an improved fuzzy clustering algorithm in SAR image change detection and used a weighted distance to reflect neighborhood pixels.[4,13] In a study by Gong et al.,[4] the Markov random field was combined with FCM to balance image details and noise. Li et al. introduced Gamma correction into fuzzy local information C-means clustering (FLICM) algorithm with better robustness.[14] Through the combination of bilateral filtering and FLICM algorithm, Shang et al.[15] have successfully accomplished precise detection and identification of potential change regions in remote sensing imagery. This study offers a novel perspective and methodology for analyzing remote sensing images, thereby making important contributions to the advancement of relevant domains.

The rise of deep learning algorithms provides a new approach to SAR image change detection. Literature[16,17] classifies hyperspectral images, and Li et al.[9] propose a lightweight network model for images. Gao et al.[18] used SAR images to detect changes in sea ice and virtual samples to enrich training samples. Li et al.[19] combine the clustering algorithm with CWNN convolution. Zhang et al.[20] integrated a convolutional wavelet neural network (CWNN) with a deep convolutional generative adversarial network. Some researchers improved the quality of training samples by utilizing information on the frequency domain of SAR images[2] and via comparisons between salient regions and neighboring pixels[20] based on the cascaded principal component analysis network (PCANet).[21]

Most deep learning methods follow the FCM clustering algorithm to generate labels; however, SAR image change detection based on FCM pre-classification produces deviations in the results.[22] The number of labels obtained with FCM clustering is relatively small and insufficient in ensuring sample input in some deep learning algorithms. At the same time, the network learns directly from the image and is affected by speckle noise, which interferes with the changing and non-changing features of pixels.

Herein, we proposed a bi-temporal SAR image change detection method for denoising an image space domain. It predominantly involves the following two aspects:

1. Inspired by Zhang et al.,[23] the fast and flexible denoising convolutional neural network (FFDNet) model is used to reduce speckle noise and real SAR images to retain the network parameters. The denoised image results agreed with direct human observation and improved the accuracy of the change detection algorithm.
2. To avoid excluding the correlation between the central and neighboring pixels in the clustering algorithm,[24] we used fuzzy local information C-means (FLICM) clustering to classify the SAR images.

2 Experimental Method

In this section, we present a comprehensive description of the methodology employed in this paper and elucidate the structure of the FFDNet model. We provide explicit clarification regarding the functions and roles of each component within the FFDNet model, along with their inherent advantages in image denoising tasks. Subsequently, we outline the formulas utilized for

calculating using differential operators. Furthermore, our focus is directed towards an extensive discussion on pivotal steps involved in fuzzy clustering. Fuzzy clustering represents an unsupervised learning approach that partitions a dataset into distinct groups based on similarity measures. Within this section, we offer a thorough exposition of fuzzy clustering algorithms encompassing mathematical principles and computational processes. Additionally, two distinct types of feature descriptions are employed to evaluate traditional datasets as well as algorithm performance indicators within this context.

2.1 Proposed Method

In this section, we present a comprehensive description of the methodology employed in this paper. The algorithm flowchart proposed by us is depicted in Fig. 1. Initially, the dual-temporal SAR images are fed into the FFDNet structure for denoising, resulting in denoised images T_1 and T_2, respectively. This algorithm effectively mitigates noise in the images and enhances the accuracy of subsequent processing steps. Subsequently, we introduce the logarithmic ratio method to generate difference operators. By calculating the logarithmic ratio between each pixel value of two images and mapping it to a new grayscale range, it can effectively emphasize areas of change while suppressing irrelevant information. Lastly, we employ a fuzzy clustering algorithm on the difference operator to derive the final change detection outcome. Fuzzy clustering is a widely adopted technique for data classification and segmentation tasks that has been applied herein to identify and label changes occurring in SAR images.

2.2 FFDNet Denoising Model

The presence of speckle noise in two-phase SAR images hampers the visualization and interpretation of ground objects by causing interference. Hence, it becomes imperative to mitigate this issue during change detection analysis. Employing speckle filtering techniques aids in achieving a smoother difference image while minimizing false alarms caused by speckle noise.

The FFDNet-based image denoising method utilizes a network to learn and subtract the noise from the original image. Unlike existing convolutional neural networks (CNNs) that primarily focus on Gaussian denoising, which lacks generalization ability for complex noise in real noisy images, Zhang et al. addressed this issue by incorporating a noise-level map as input. In order to better handle speckle noise in SAR images, this study employed speckle noises as retraining samples to design a CNN-based noise model specifically tailored for SAR images. By processing the downsampling operator, a wider range of noise was effectively eliminated.

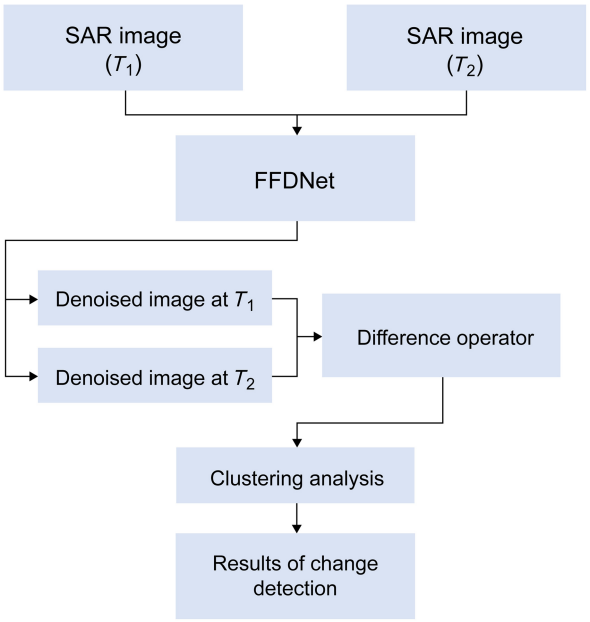

Fig. 1 Overall design process of this experiment.

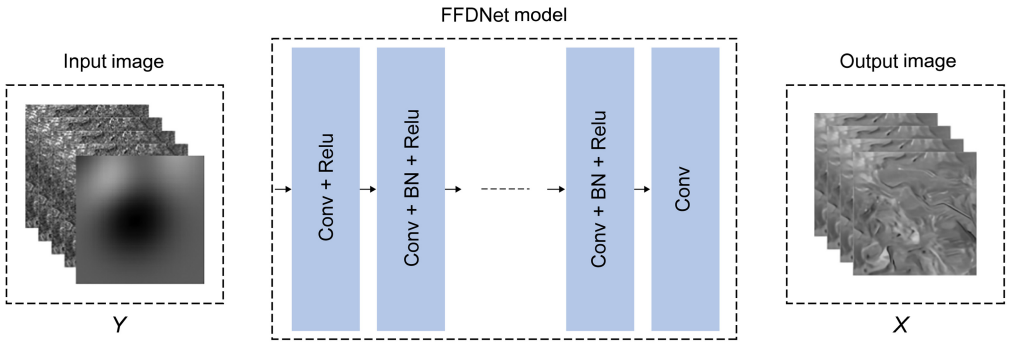

Fig. 2 Architecture of the fast and flexible denoising convolutional neural network for image denoising. BN, batch normalization; Conv, convolution; ReLU, rectified linear unit.

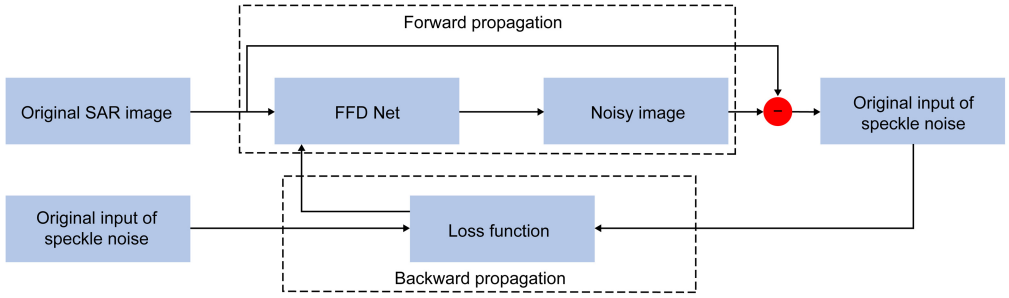

Fig. 3 Fast and flexible denoising convolutional neural network architecture used for image denoising.

The network structure depicted in Fig. 2 took the original real SAR image with speckle noise as input, and the training process is illustrated in Fig. 3.

The input Y comprised reversible downsampling operators that reshaped the input image into four downsampled sub-images. These were then input into the convolution together with the noise-level images. The noise-level images assign a specific noise level to each pixel of an image to balance between noise reduction and detail preservation in the presence of spatially varying noise.[17–19] The size of the input image Y was defined as $W \times H \times C$; the size of the downsampled sub-images was $W/2 \times H/2 \times 4C$, where C is the number of channels of the image, designated as 1 in the SAR denoising model; the sub-images were connected with the noise-level images as a tensor of $W/2 \times H/2 \times (4C + 1)$, which was used as the CNN data input.

CNN is composed of a series of 3×3 convolutional layers, with the first convolutional layer in "Conv + ReLU," the middle 15 layers in "Conv + BN + ReLU," and the last layer in "Conv." The feature map was filled with zeros to retain its constant size.

Reconstructed from the output X were four sub-images that had undergone denoising, resulting in the restoration of the original denoised image. Following FFDNet,[23] this study employed a SAR grayscale image for denoising; specifically, the parameters for grayscale image convolution layers, grayscale image feature map channels, and downsampling factor were set at 15, 64, and 2 respectively. The SAR input image was normalized without introducing additional errors in the calculation or changing the information stored in the image. The original image was then compressed to the range of 0 to 1 using

$$\text{norm} = \frac{y_i - \min(y)}{\max(y) - \min(y)}. \tag{1}$$

In the forward propagation, FFDNet uses residual learning to train a residual map, as shown

$$R(y_i; \lambda) \approx y_i - x_i, \tag{2}$$

where $R(y_i;\lambda)$ is the noisy image predicted by the network, λ is the training network parameters, y_i is the original noisy input image, and x_i is the noise-free label map.

In the backward propagation, the mean square error was used as the loss function, as shown in Eq. (3), and the adaptive moment estimation algorithm was used to minimize the loss function

$$\partial(\lambda) = \frac{1}{2N}\sum_{i=1}^{N}\|x_i - x_i\|^2, \tag{3}$$

$$x_i = y_i - R(y_i - x_i), \tag{4}$$

where N is the number of training samples.

After training the network using SAR images containing speckle noise, the trained FFDNet was utilized to denoise real datasets with updated network parameters. Consequently, the original image was restored from the four sub-images generated through downsampling.

2.3 Difference Operators

Difference image (DI) generation was used to identify the differences between the two images with a specific calculation method to reflect the changed parts of the SAR images.[20] Accordingly, this section introduces the difference operators applied in the experiments mentioned in Sec. 3.

The subtraction operator obtains the DI by directly subtracting the two images, as shown in Eq. (5). Given that the pixel value cannot be negative, X in the difference calculation is defined as the absolute value of the subtraction of the two images. Earlier studies have used the difference method owing to its simple concept and implementation. However, this method cannot effectively remove coherent speckle noise. Therefore, it has subsequently been improved by researchers

$$X = |X_2 - X_1|. \tag{5}$$

The log-ratio (LR) operator adds logarithmic operations into the ratio method that transforms the multiplicative noise model into an additive noise model,[2] as expressed in Eq. (6). This method is widely used in DI acquisition. However, the logarithmic operation enhances the shrinkage of the pixels to ensure that the edge pixel details cannot be well preserved or may be blurred

$$X_{\mathrm{LR}} = \left|\log\frac{X_2}{X_1}\right| = |\log X_2 - \log X_1|, \tag{6}$$

where X_2 and X_1 are the input image information, and the gray value in the SAR image matrix is applied to the calculation.

In the real calculations, to avoid calculation errors caused by zero-pixel values in the image X_{LR}, 1 is added to the pixel values calculated in Eq. (6) to obtain the logarithmic ratio operator using Eq. (7) as follows. This differential operator has been chosen as the preferred method in our study presented in this article.

$$D_L = \left|\log\frac{X_2+1}{X_1+1}\right| = |\log(X_2+1) - \log(X_1+1)|. \tag{7}$$

The mean-ratio (MR) uses the neighborhood information of the pixel, expressed in Eq. (8), and replaces the texture feature or gray value of the corresponding pixel with the mean value of the neighborhood pixels of the pixel point. This method can suppress the coherent speckle in the form of a single pixel point

$$X_{\mathrm{MR}} = 1 - \min\left(\frac{X_2}{X_1}, \frac{X_1}{X_2}\right). \tag{8}$$

Rezaei and Karami demonstrated that the noise in SAR images is speckle noise.[21] In this study, the ideal LR and MR were selected as the difference operators in the experiment.

In the experimental analysis, we conducted a comparative study of various difference operators and established objective criteria for their mutual evaluation. These comparisons enable us to comprehensively assess and comprehend the performance of different difference operators in specific contexts. Our experimental analysis revealed that each difference operator possesses

unique advantages and limitations when applied to data processing. Certain operators exhibit suitability for specific types or smaller-scale datasets, excelling in extracting crucial information. Conversely, others are better suited for handling large-scale complex datasets, offering advantages in terms of stability and accuracy maintenance.

2.4 FLICM Algorithms

Krinidis and Chatzis improved the FCM algorithm and proposed the FLICM algorithm by incorporating local and sample spatial information and the gray values of the images, which increases the robustness of the sample application.[22]

The objective function of the FLICM algorithm is shown as

$$J = \sum_{i=1}^{n} \sum_{k=1}^{c} u_{ki}^{m} \|x_i - v_k\|^2 + G_{ki}, \tag{9}$$

where the existing image has n pixel points; the i'th pixel is x_i; the number of cluster center categories is c; $\|x_i - v_k\|^2$ is the Euclidean distance between sample point x_i and the cluster center v_i; u_{ki} is the membership degree of the sample point relative to the cluster center; m is the membership degree weight of the sample point to the cluster center that is usually set to 2, according to the experiment by Hwang and Haddad[23]; and G_{ki} is the fuzzy factor.

The fuzzy factor is shown as

$$G_{ki} = \sum_{x_j \in N_i} \frac{1}{d_{ij} + 1} (1 - u_{kj})^2 \|x_i - v_k\|^2, \tag{10}$$

where N_i is the set of neighborhood pixels X_j; the neighborhood window of the pixels x_i to be classified is 3×3; d_{ij} is the Euclidean distance between x_j and x_i; and u_{kj} denotes the membership degree of the neighborhood pixels x_j to the cluster center v_k.

Derived from the Lagrange multiplier method, the membership degree u_{kj} to the cluster center v_k is obtained by an iterative calculation to minimize the objective function, as shown

$$u_{ki} = \frac{1}{\sum_{j=1}^{c} \left(\frac{\|x_i - v_k\|^2 + G_{ki}}{\|x_i - v_j\|^2 + G_{ji}} \right)^{\frac{1}{m-1}}}, \tag{11}$$

$$v_k = \frac{\sum_{i=1}^{N} u_{ki}^{m} x_i}{\sum_{i=1}^{N} u_{ki}^{m}}. \tag{12}$$

The fuzzy factor introduced in the FLICM algorithm accounts for the spatial and gray value relationship between pixels. Compared with the original FCM algorithm, it saves computational time and reduces the outline blurring of the changing subject in the SAR gray image.

2.5 Experimental Data

To verify the effectiveness of the experimental protocol, we selected two sets of real data for comparison. The study areas and change reference image are shown in Fig. 4. The first set of experimental data, 301×301 pixels in size, were SAR images captured by the European

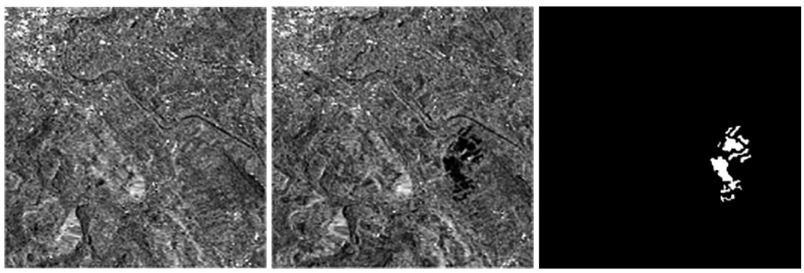

Fig. 4 Synthetic aperture radar image of the Bern area, Switzerland. (a) April 1999; (b) May 1999; (c) Change reference image of Figs. 4(a) and 4(b).

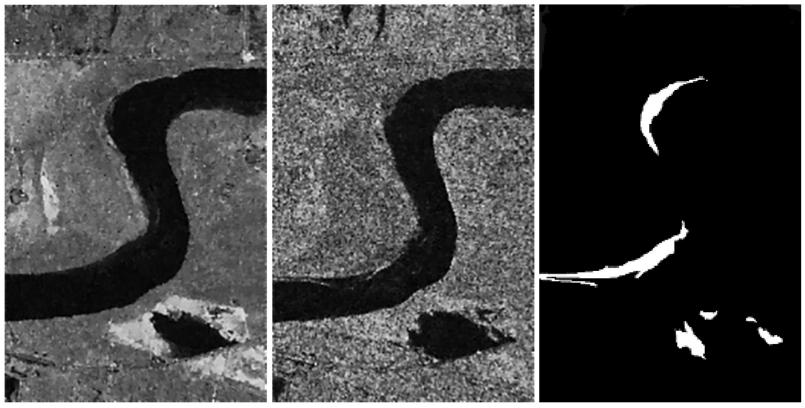

Fig. 5 Synthetic aperture radar image of the Yellow River area. (a) June 2008; (b) June 2009; (c) Change reference image of Figs. 5(a) and 5(b).

Remote Sensing Satellite-2 of Bern, Switzerland. Images in Figs. 4(a) and 4(b) were captured in April and May 1999, respectively; they show the flood situation near the suburbs of Bern, where Fig. 4(c) is the change reference image.

The resolution of the second experimental dataset was 444×291 pixels, which was captured by the Radarsat-2 SAR satellite. Figures 5(a) and 5(b) show the inland waters of the Yellow River in China in June 2008 and June 2009, respectively. Figure 5(c) is the change reference image. Changes occurred predominantly at the riverbanks.

2.6 Evaluation Metrics

Change detection is predominantly used to recognize changed and unchanged pixels, quantitatively evaluate the performance of the SAR image change detection algorithm and verify the effectiveness of an algorithm via objective analysis of the experimental results. To assess its accuracy, the five evaluation indicators in this study were false negatives (FN), false positives (FP), overall errors (OE), percentage correct classification (PCC), and the Kappa coefficient. FN indicates the number of changed pixels classified as non-changed, FP denotes the number of non-changed pixels classified as changed, OE is the sum of FN and FP, and PCC indicates the ratio of correct detections to total pixels. The Kappa coefficient is an important evaluation indicator that considers the correctly and falsely detected pixels. When the value is closer to 1, the detection effect is more effective.

The calculations for the PCC and Kappa coefficient are shown in Eq. (13) and (14) below, respectively:

$$\mathrm{PCC} = \frac{\mathrm{Num} - \mathrm{OE}}{\mathrm{Num}}, \tag{13}$$

$$\begin{cases} \mathrm{Kappa} = \frac{\mathrm{PCC}-P}{1-P} \\ P = \frac{\mathrm{TP}+\mathrm{FN}}{\mathrm{Num}} \times \frac{\mathrm{TP}+\mathrm{FP}}{\mathrm{Num}} + \frac{\mathrm{TN}+\mathrm{FP}}{\mathrm{Num}} \times \frac{\mathrm{TN}+\mathrm{FN}}{\mathrm{Num}} \end{cases}, \tag{14}$$

where Num indicates the total number of image pixels, TP denotes the number of changed pixels classified as changed, and TN represents the number of non-changed pixels classified as non-changed.

In this study, the peak signal-to-noise ratio (PSNR) and structural similarity index (SSIM) were used for the DI analysis.[25] PSNR was used to measure the differences between the two images and calculate the degree of difference between the images. The minimum value of PSNR is 0; when PSNR is larger, the difference between the two images is larger. The minimum and maximum values of SSIM are 0 and 1, respectively. When SSIM is larger, the two images are more similar.

3 Results

To validate the effectiveness of the change detection algorithm after DI denoising, we conducted experiments on the two abovementioned sets of real data. The images were preprocessed with the FFDNet model to denoise the DI and improve their quality. Subsequently, the LR operator was constructed with the denoised bi-temporal image, and its quality was evaluated. The DIs were classified using fuzzy clustering to generate the final change detection result map.

3.1 Quality Assessment of Difference Operators

To verify the effectiveness of the difference operators, we conducted experiments on the quality of the operators, and the PSNR and SSIM values of the original image were calculated. Figures 6 and 7 show the denoising results of the Bern and Yellow River datasets, respectively. These results indicate that the speckle noise in the images has been substantially suppressed, and the overall image is more uniform.

Tables 1 and 2 show the PSNR and SSIM values of the datasets, where a is the image of the first phase and the result after the first phase of denoising, and b is the image of the second phase and the result after the second denoising phase.

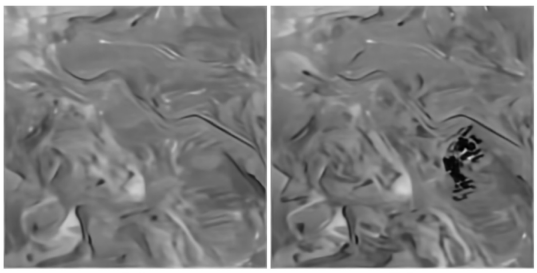

(a) (b)

Fig. 6 Denoised image of the Bern region. (a) Image denoising results before floods; (b) Image denoising results after floods.

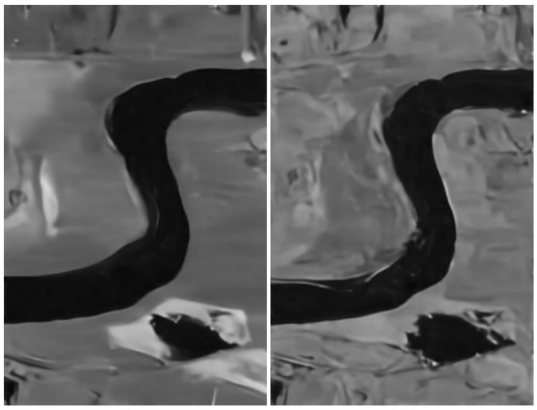

(a) (b)

Fig. 7 Denoised image of the Yellow River region. (a) Noise removal results before riverbank change; (b) Noise removal results after riverbank change.

Table 1 Evaluation index of various difference operators in the Bern region.

	SSIM[a]	PSNR[b]
a	0.3424	19.5675
b	0.4019	20.1387

[a]Structural similarity index.
[b]Peak signal-to-noise ratio.

Table 2 Evaluation index of various difference operators in the Yellow River region.

	SSIM[a]	PSNR[b]
a	0.5188	23.6021
b	0.3476	17.9258

[a]Structural similarity index.
[b]Peak signal-to-noise ratio.

Table 3 Evaluation index of various difference operators in the Yellow River region.

	SSIM[a]	PSNR[b]
Sub-log[c]	0.0138	19.1353
Sub-MR[d]	0.0363	19.3952
Sub-proposed[e]	0.0094	19.0732
Log-proposed[e]	0.9941	57.9231

[a]Structural similarity index.
[b]Peak signal-to-noise ratio.
[c]Sub-log, the comparison between the difference operator and logarithmic ratio operator.
[d]Sub-MR, the comparison between the difference operator and mean ratio operator.
[e]Sub-proposed and log-proposed, the comparison between the corresponding operator and the operator proposed in this study.

Table 4 Evaluation index of various difference operators in the Bern region.

	SSIM[a]	PSNR[b]
Sub-log[c]	0.1907	18.7553
Sub-MR[d]	0.1959	18.8865
Sub-proposed[e]	0.1836	18.6966
Log-proposed[e]	0.9939	57.3823

[a]Structural similarity index.
[b]Peak signal-to-noise ratio.
[c]Sub-log, the comparison between the difference operator and logarithmic ratio operator.
[d]Sub-MR, the comparison between the difference operator and mean ratio operator.
[e]Sub-proposed and log-proposed, the comparison between the corresponding operator and the operator proposed in this study.

The evaluation metrics of the original images were calculated using different difference operators, as shown in Tables 3 and 4. These compare the difference operator with the LR operator, mean ratio, and operator after FFDNet noise reduction. The results between the conventional and LR operator proposed in this paper were obtained. In terms of PSNR, the LR and DI after FFDNet denoising were three-fold that of the original, and the SSIMs all exceeded 0.99. The objective indicators showed that most of the similarities in the LR and DI remain unchanged.

3.2 Change Detection Results and Analysis

The method proposed in this study is referred to as FFDNet-F. The experimental results of the Bern dataset are shown in Fig. 8 and Table 5.

Fig. 8 Change detection results obtained using different methods for multi-temporal images of Bern. (a) K-means, algorithms for hard clustering; (b) fuzzy C-means; (c) principal component analysis; (d) principal component analysis network; (e) capsule network; (f) convolutional wavelet neural network; (g) fast and flexible denoising convolutional neural network, the method proposed in this study.

Table 5 Metrics of the Bern dataset.

Kappa	PCC	FP	FN	OE	Method
70.35	99.24	360	326	686	K-means
62.29	99.21	162	554	716	FCM
85.75	99.64	179	150	329	PCAKM
75.37	99.49	434	31	465	PCANet
76.29	99.45	172	329	501	CapsNet
85.28	99.65	85	230	315	CWNN
83.58	99.62	95	254	349	FFDNet-F

K-means[26] and FCM clustering[27] algorithms exhibited low overall Kappa coefficients in the Bern dataset and produced more speckle noise in the image, which resulted in a substantial number of false alarms. The principal component analysis and K-means clustering (PCAKM) algorithm[28] reduced noise by selecting the dimension of the feature space to ensure that the edge of the image is smooth and the outline of the changing subject is distinct. PCANet[23] demonstrated a pronounced effect in terms of suppressing speckle noise after pre-classification.[9] The accuracy of the results of PCANet was higher than that of the results of the classic clustering K-means and FCM methods, with the original Kappa value increasing by 5.02 and 13.08, respectively. However, owing to a higher FP, some content was missing, and the Kappa coefficient was lower for the PCANet results than that for the PCAKM results. CapsNet used the adaptive fusion convolution module and improved the accuracy of the results via feature conversion.[3] The CWNN method has been applied in sea ice detection[19]; however, the Kappa coefficient was higher in the flooded area in the Bern dataset. The method used in this study produced a lower Kappa coefficient than those of the PCAKM and CWNN in the Bern dataset, respectively. However, the accuracy of the results improved substantially compared with that of the other methods used in the study.

The experimental results from the Yellow River and Bern datasets are shown in Fig. 9 and Table 6.

The K-means[26] and FCM clustering[27] algorithms in the Yellow River dataset had an overall lower Kappa coefficient. The FCM clustering algorithm had a high FP value and prominent noise, with a Kappa coefficient of 16.98. The PCAKM algorithm enriched the details of the changing subject, and the outline was more distinct.[28] PCANet had a lower Kappa coefficient than that of PCAKM[23]; however, the Kappa coefficient improved by 2.6%. CapsNet reduced false alarms, and its Kappa coefficient improved by 2.66%[3]; therefore, the Kappa coefficient was higher than that of PCANet. CWNN had a low FN value.[19] The methods used in this study demonstrated the highest accuracy for the Yellow River dataset, and the accuracy of the results was considerably enhanced.

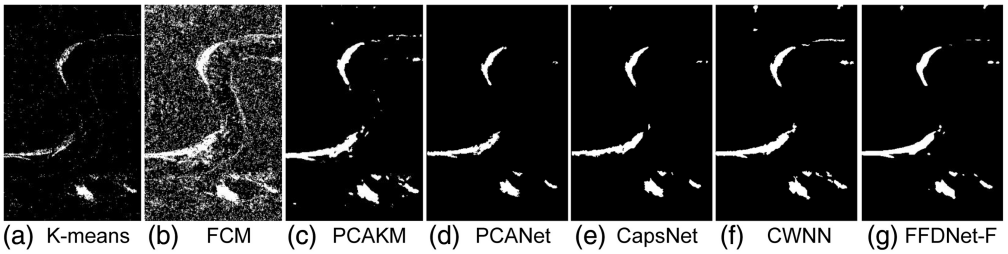

Fig. 9 Change detection maps obtained using different methods for multi-temporal images of the Yellow River. (a) K-means, algorithms for hard clustering; (b) fuzzy C-means; (c) principal component analysis; (d) principal component analysis network; (e) capsule network; (f) convolutional wavelet neural network; (g) fast and flexible denoising convolutional neural network, the method proposed in this study.

Table 6 Metrics of the Yellow River dataset.

Kappa	PCC	OE	FN	FP	Method
53.70	96.72	4232	1629	2603	K-means
16.98	79.17	26912	510	26402	FCM
74.66	98.20	2325	657	1668	PCAKM
77.26	98.54	1887	677	1210	PCANet
79.92	98.29	2207	1468	739	CapsNet
78.34	98.46	1990	483	1507	CWNN
82.05	98.63	1765	624	1141	FFDNet-F

Given that traditional clustering methods like K-means and FCM only consider individual pixels without taking into account other spatial data, they are highly sensitive to image noise and can potentially introduce more overall noise. Although these methods may achieve local optimization, they have certain global limitations. In recent years, the field of image processing has introduced deep learning techniques such as PCANet. These approaches view clustering as preclassification and optimize sample labels, which are closely related to sample quality, thereby improving clustering performance. Deep learning techniques effectively utilize feature information within images while demonstrating robustness and generalization capabilities compared to conventional methods. This study combines deep neural networks with FLICM clustering methodology and validates its effectiveness through experimental results.

In this study, we propose a new method that combines deep neural networks with fuzzy local information C-means (FLICM) clustering. The experimental results demonstrate the effectiveness of this approach in utilizing the advanced capabilities of deep neural networks for extracting and representing features, while also incorporating spatial relationship information considered by the FLICM algorithm to accurately model data distribution. By simultaneously optimizing network parameters and sample labels, our method improves both accuracy and robustness in image clustering tasks based on the FLICM algorithm.

3.3 Window Parameter Experiment

The window parameters for clustering, based on different neighborhoods, specifically impacted the experimental results and produced a sharpening or smoothing effect. The window parameters involved in the FLICM algorithm were examined when set to 3, 5, 7, 9, and 11. The results of the Bern dataset are shown in Fig. 10, and those of the Yellow River dataset are shown in Fig. 11.

The experimental results show that the window value in clustering specifically influenced detection result accuracy. As the window value increased, the outline of the main changing

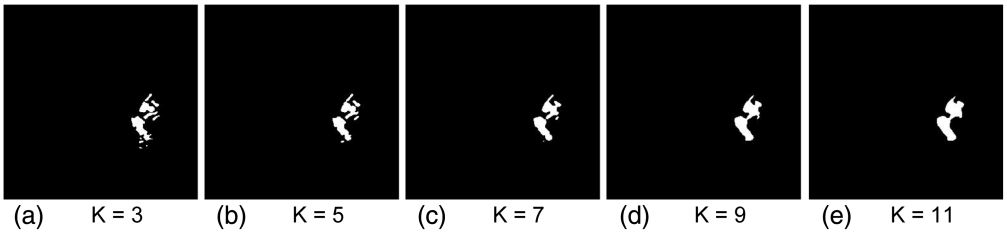

Fig. 10 Bern dataset results for different window values. K, window size.

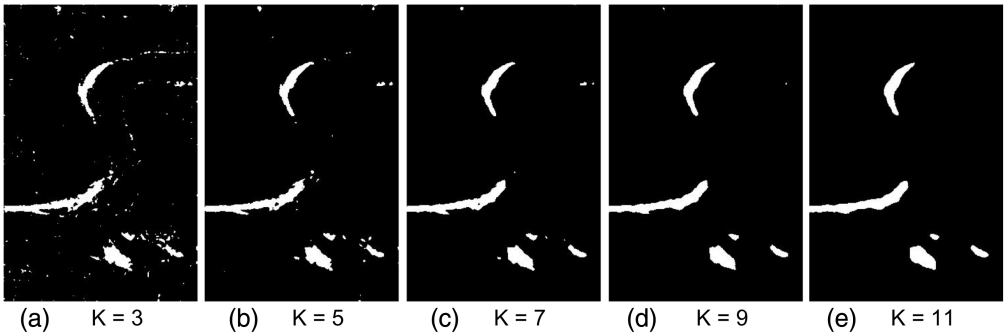

Fig. 11 Yellow River dataset results for different window values. K, window size.

Table 7 Kappa values in different windows.

Kappa	$K = 3$	$K = 5$	$K = 7$	$K = 9$	$K = 11$
Bern	**85.46**	83.58	80.07	77.06	74.11
Yellow River	80.81	82.05	**82.21**	81.45	80.89

subject in the detection smoothened. In the results, the discrete points of the lake gradually converged with the main part as the window value increased, and the resulting fragmentation traces were weakened. The main body of results from the Bern dataset tends to comprise one area, whereas the Yellow River dataset comprises three parts (Figs. 10 and 11, respectively). The Kappa value and PCC under different windows are shown in Table 7 and Fig. 12.

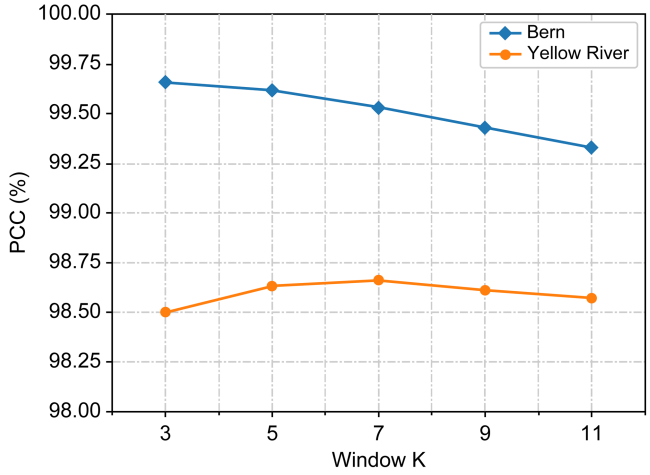

Fig. 12 Relationship between the size of the window and the percentage correct classification in the two datasets.

The Kappa and PCC values in the Bern dataset (Fig. 10) gradually decreased with increasing window values; there was a pronounced degree of decline. The two indicators in the Yellow River dataset (Fig. 11) reached extreme values when the window was set to 7, and the overall level was less affected by the window value.

3.4 Real Data Verification

To verify the effectiveness of the method, we used China's GF-3 satellite data for verification and selected a typical flood region. We chose Zhengzhou city, China, which suffered major floods in July 2021. The two Zhengzhou flood datasets, A and B, represent different regions during flood occurrence. Both sets were collected by GF-3 on July 20 and July 24, 2021 (resolution: 5 m). Dataset A showed the changes during inland floods, with significant widening on both sides of the river and relatively concentrated waterlogging areas. Dataset B showed marginal water body fading and inland farmland water body irrigation changes. The changed features were relatively fragmented.

In the Zhengzhou flood datasets, as shown in Figs. 13 and 14, the overall detection accuracy of the clustering algorithm was relatively low. In particular, the Kappa coefficient of the FCM algorithm did not exceed 50, representing a significant amount of error detection. The deep learning method represented by PCANet significantly improved the accuracy of change detection.

For Zhengzhou dataset A, the FCM algorithm resulted in a large number of noise points, while the CapsNet method achieved the highest accuracy (Fig. 15 and Table 8). The method in this study detects more discrete non-changing regions and classifies a small portion of the noise as changing parts. In Zhengzhou dataset B, the results in Fig. 16 and Table 9 show that the detection accuracy of the FCM algorithm was still relatively low, while the detection accuracy of the CWNN algorithm decreased significantly. The method in this study suppresses noise in advance, resulting in generally stable detection accuracy.

In the experimental method, the efficacy of the K-means and FCM clustering algorithms in the Bern dataset is constrained, as indicated by their relatively low overall Kappa coefficients.

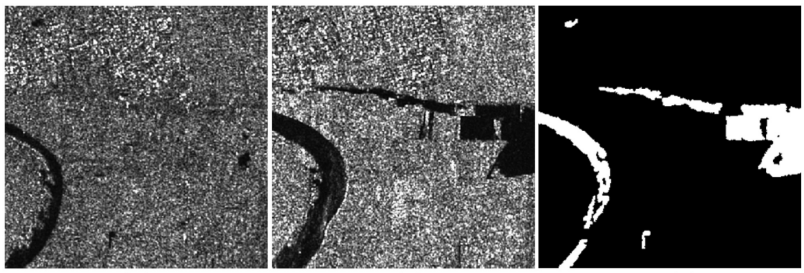

Fig. 13 Synthetic aperture radar image of the Zhengzhou area, China, using dataset A from GF-3. (a) July 20, 2021; (b) July 24, 2021; (c) Change reference image of (a) and (b).

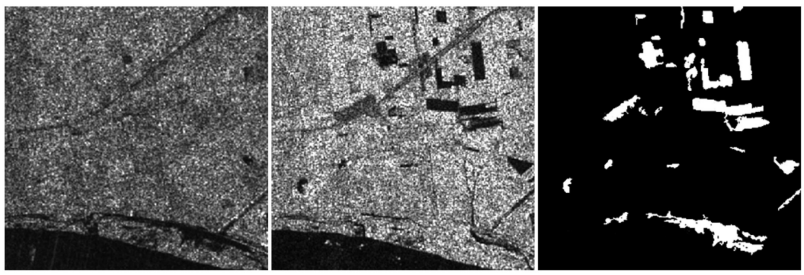

Fig. 14 Synthetic aperture radar image of the Zhengzhou area, China using dataset B from GF-3. (a) July 20, 2021; (b) July 24, 2021; (c) Change reference image of (a) and (b).

Fig. 15 Change detection maps obtained for multi-temporal images of the Yellow River using different methods. (a) *K*-means, algorithms for hard clustering; (b) fuzzy C-means; (c) principal component analysis; (d) principal component analysis network; (e) capsule network; (f) convolutional wavelet neural network; (g) fast and flexible denoising convolutional neural network, the method proposed in this study.

Table 8 Metrics of Zhengzhou Dataset A.

Kappa	PCC	OE	FN	FP	Method
62.4	93.32	6016	2912	3104	K-means
43.05	84.16	14258	1420	12838	FCM
83.58	97.38	2357	2106	251	PCAKM
74.59	96.29	3343	3343	0	PCANet
88.8	98.1	1713	1199	514	CapsNet
85.28	97.68	2086	2083	3	CWNN
83.28	97.27	2456	1946	510	FFDNet-F

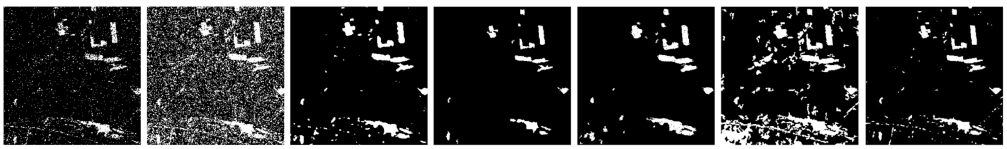

Fig. 16 Change detection maps obtained for multi-temporal images of the Yellow River using different methods. (a) *K*-means, algorithms for hard clustering; (b) fuzzy C-means; (c) principal component analysis; (d) principal component analysis network; (e) capsule network; (f) convolutional wavelet neural network; (g) fast and flexible denoising convolutional neural network, the method proposed in this study.

Table 9 Metrics of Zhengzhou Dataset B.

Kappa	PCC	OE	FN	FP	Method
48.75	93.39	5951	3252	2699	K-means
23.31	75.87	21719	1368	20351	FCM
72.52	96.6	3061	2084	977	PCAKM
59.4	95.85	3737	3553	184	PCANet
73.13	96.73	2941	2138	803	CapsNet
51.19	89.65	9312	568	8744	CWNN
71.71	96.46	3187	2255	932	FFDNet-F

Moreover, these algorithms tend to introduce a higher level of speckle noise into the image, leading to a considerable number of false alarms.

The PCAKM algorithm addresses the issue of noise by meticulously selecting the dimension of the feature space, ensuring not only a smooth image edge but also distinct outlines for any changing subject within it. This approach effectively minimizes false alarms caused by excessive speckle noise. By incorporating principal component analysis into the clustering process, PCAKM successfully reduces noise while preserving crucial features in an image. The careful selection of appropriate dimensions for feature extraction enables improved discrimination between different regions or objects within an image.

PCANet leverages the neighborhood features encompassing each pixel to extract valuable information from images. Through meticulous analysis and comparison of individual pixels, PCANet effectively captures the correlations and similarities between diverse regions within the image. In contrast to alternative approaches, PCANet exhibits remarkable robustness in handling speckle noise. As a method for extracting neighborhood features, it demonstrates exceptional resilience in mitigating speckle noise while achieving the lowest FN value.

CapsNet employs a multi-scale capsule module for effectively modeling the spatial relationship between objects. This module exhibits the capability to capture objects at various scales and aggregate them to obtain comprehensive global information. By aggregating features from diverse positions, we are able to holistically consider information from each position, thereby significantly improving change detection accuracy. Notably, this approach has demonstrated remarkable detection accuracy across multiple datasets in empirical evaluations.

CWNN algorithm utilizes wavelet transform to reduce the impact of speckle noise in SAR images. By incorporating wavelet transform, CWNN effectively reduces the blurring effects caused by speckle noise in SAR images. Additionally, during training, CWNN employs a method for generating virtual samples as an extra strategy. This approach successfully tackles the challenge posed by limited training samples and greatly improves detection accuracy.

4 Discussion

The original SAR image obtained after satellite signal interpretation contained speckle noise. Errors in signal processing and transmission in each band may cause some interference in the acquired image and alter the result. Although we suppressed speckle noise to some extent, the quality of the SAR images remained uncertain. The source of SAR image samples for noise suppression and the superposition of multiple noises in the images are possible uncertainty factors. Considering noise suppression, FFDNet-F has substantial advantages over clustering and deep neural network methods. The resolution of SAR images can be further improved using multidimensional and multi-domain features of SAR images, including time, frequency, spatial, time-frequency, and transform domains. Simultaneously, pre-classification or secondary classification clustering and other algorithms can still be improved.

As shown in the spatial denoising results in Figs. 6 and 7, the surface noise was smoothened, and the primary water body system was highlighted. The contrast between the two areas is distinct, indicating that the speckle noise was suppressed.

Two clustering algorithms discretized the changed ground objects in the results and cut the original ground morphology to a certain extent (Figs. 8 and 9). PCAKM, PCANet, CapsNet, CWNN, and FFDNet-F methods retain the original surface morphology to the fullest extent, and the changed results are distinct.

The FLICM algorithm was analyzed using the window parameter, K, in the clustering algorithm, as shown in Figs. 10 and 11. The Bern dataset was greatly affected by the window neighborhood in the window selection. Our analysis determined that the main changes in the Bern dataset were concentrated in the lower right image segment. Most areas in the image did not change during the neighborhood search, indicating that detection accuracy substantially decreases when the neighborhood is expanded. The changed areas in the Yellow River dataset were evenly distributed. Adjusting the window parameter, K, minimally affected the overall progress. Table 7 and Fig. 12 validate our analysis.

The results based on real images in recent years have shown that reducing speckle noise in advance can greatly improve detection accuracy. The Zhengzhou data mainly captures farmland; owing to the impact of surface crops, farmland data can generate a large amount of speckle noise, which may cause confusion in the results. The FFDNet-F algorithm is not only applicable to the older Bern and Yellow River datasets but also demonstrates good operational results in the new high-degree series of satellite datasets. The method of suppressing speckle noise in advance has also been analyzed.

This study focuses on the means of change detection in the spatial domain. Simultaneously, the noise reduction algorithm in the human visual domain (spatial domain) is maturing, which benefits from the timely quality control feedback in the algorithm process. The details cannot be directly observed in other domains, such as the frequency domain, resulting in less use of each link in the change detection algorithm; however, the overall accuracy can be improved using the information on the domain. The use of information in multiple dimensions and domains can be improved.

Most of the datasets used by the algorithms in the industry are small-sample SAR images, and the calculation rate is substantially reduced for larger images. Improving the detection accuracy for small samples is crucial; however, the image cannot adhere to the requirements of overall judgment after clipping. A decreased detection speed causes the algorithm to be less efficient than manual observation, and a quicker speed needs to maintain a certain degree of accuracy. Limited by the quality of data samples, this study used a small range of sample sets. The FFDNet used for noise reduction in this study uses the FLICM algorithm for classification, which is faster than the overall neural network method but has accuracy flaws.

5 Conclusions

The presence of speckle noise has a significant impact on the outcomes of change detection in SAR images. To enhance the accuracy of results, it is crucial to reduce the inherent levels of speckle noise within these images. The preservation of data integrity in areas undergoing changes can be achieved by employing an appropriate denoising model. In this research, we have effectively utilized the FFDNet architecture to decrease speckle noise while also implementing FLICM clustering with fuzzy factors to further mitigate its impact. Our experiments demonstrate improved Kappa values within evaluation indices and successfully achieve a balanced representation across both Bern and Yellow River datasets.

Furthermore, in recent evaluations conducted on the dataset of the Zhengzhou flood disaster, this algorithm exhibited exceptional performance and demonstrated remarkable precision in detection. This implies that we can more accurately identify flood-related information and promptly implement response measures.

Disclosures

The authors declare no potential competing interests.

Code and Data Availability

We used the experimental data of Professor Gao's team. The data used in this study can be found in the following link: feng-gao.cn.

Author Contributions

Conceptualization: Yuqing Wu and Qing Xu; data curation: Yuqing Wu, Qing Xu, Xinming Zhu, and Tianming Zhao; formal analysis: Yuqing Wu, Qing Xu, and Jingzhen Ma; investigation: Yuqing Wu, Xinming Zhu and Tianming Zhao; methodology: Yuqing Wu and Qing Xu; writing – original draft: Yuqing Wu and Qing Xu; writing – review & editing: Bowei Wen and Jingzhen Ma.

Acknowledgments

This research was funded by the Young Scientists Fund of the National Natural Science Foundation of China [grant number 42101455], the National Natural Science Foundation of China [grant number 42101454], the Zhongyuan Scholar Program of Henan Province [grant

number 202101510001], the Joint Fund of Collaborative Innovation Center of Geo-Information Technology for Smart Zhongyuan, Henan Province, and the Key Laboratory of Spatiotemporal Sensing and Intelligent processing, Ministry of Natural Resources [grant number 212102].

References

1. M. Gong, H. Yang, and P. Zhang, "Feature learning and change feature classification based on deep learning for ternary change detection in SAR images," *ISPRS J. Photogramm. Remote Sens.* **129**, 212–225 (2017).
2. X. Qu et al., "Change detection in synthetic aperture radar images using a dual-domain network," *IEEE Geosci. Remote Sens. Lett.* **19**, 4013405 (2022).
3. Y. Gao et al., "SAR image change detection based on multiscale capsule network," *IEEE Geosci. Remote Sens. Lett.* **18**(3), 484–488 (2021).
4. M. Gong, Z. Zhou, and J. Ma, "Change detection in synthetic aperture radar images based on image fusion and fuzzy clustering," *IEEE Trans. Image Process.* **21**(4), 2141–2151 (2012).
5. O. Yousif and Y. Ban, "Improving urban change detection from multitemporal SAR images using PCA-NLM," *IEEE Trans. Geosci. Remote Sens.* **51**(4), 2032–2041 (2013).
6. L. Li et al., "A novel approach for multi-focus image fusion based on SF-PAPCNN and ISML in NSST domain," *Multimedia Tools Appl.* **79**(33), 24303–24328 (2020).
7. L. Liu et al., "SAR image change detection based on mathematical morphology and the K-means clustering algorithm," *IEEE Access* **7**, 43970–43978 (2019).
8. F. Gao et al., "Synthetic aperture radar image change detection based on frequency-domain analysis and random multigraphs," *Appl. Remote Sens.* **12**(1), 016010 (2018).
9. L. Li, H. Ma, and Z. Jia, "Multiscale geometric analysis fusion-based unsupervised change detection in remote sensing images via FLICM Model," *Entropy* **24**(2), 291 (2022).
10. H. Su et al., "Nonlocal feature learning based on a variational graph auto-encoder network for small area change detection using SAR imagery," *ISPRS J. Photogramm. Remote Sens.* **193**, 137–149 (2022).
11. M. N. Ahmed et al., "A modified fuzzy c-means algorithm for bias field estimation and segmentation of MRI data," *IEEE Trans. Med. Imaging* **21**(3), 193–199 (2002).
12. F. Gao et al., "Change detection from synthetic aperture radar images based on neighborhood-based ratio and extreme learning machine," *J. Appl. Remote Sens.* **10**, 046019 (2016).
13. C. Wang et al., "Fuzzy C-means clustering with weighted energy function in MRF for image segmentation," in *IEEE Int. Conf. Fuzzy Syst. (FUZZ-IEEE)*, IEEE, pp. 210–215 (2014).
14. L. Li, H. Ma, and Z. Jia, "Gamma correction-based automatic unsupervised change detection in SAR images via FLICM model," *J. Indian Soc. Remote Sens.* **51**(5), 1077–1088 (2023).
15. R. Shang et al., "Synthetic aperture radar image change detection based on improved bilateral filtering and fuzzy C mean," *Appl. Remote Sens.* **10**(4), 046017 (2016).
16. Y. Gao et al., "Hyperspectral and multispectral classification for coastal wetland using depthwise feature interaction network," *IEEE Trans. Geosci. Remote Sens.* **60**, 1–15 (2022).
17. X. Zhang et al., "Hyperspectral pathology image classification using dimension-driven multi-path attention residual network," *Expert Syst. Appl.* **230**, 120615 (2023).
18. F. Gao et al., "Sea ice change detection in SAR images based on convolutional-wavelet neural networks," *IEEE Geosci. Remote Sens. Lett.* **16**(8), 1240–1244 (2019).
19. L. Li, H. Ma, and Z. Jia, "Change detection from SAR images based on convolutional neural networks guided by saliency enhancement," *Remote Sens.* **13**(18), 3697 (2021).
20. X. Zhang et al., "Robust unsupervised small area change detection from SAR imagery using deep learning," *ISPRS J. Photogramm. Remote Sens.* **173**, 79–94 (2021).
21. M. Li et al., "SAR image change detection using PCANet guided by saliency detection," *IEEE Geosci. Remote Sens. Lett.* **16**(3), 402–406 (2019).
22. F. Gao et al., "Automatic change detection in synthetic aperture radar images based on PCANet," *IEEE Geosci. Remote Sens. Lett.* **13**(12), 1792–1796 (2016).
23. Z. Kai, W. Zuo, and Z. Lei, "FFDNet: toward a fast and flexible solution for CNN-based image denoising," *IEEE Trans. Image Process.* **27**(9), 4608–4622 (2018).
24. K. He, J. Sun, and X. Tang, "Guided image filtering," *IEEE Trans. Pattern Anal. Mach. Intell.* **35**, 1397–1409 (2013).
25. Z. Wang et al., "Image quality assessment: from error visibility to structural similarity," *IEEE Trans. Image Process.* **13**(4), 600–612 (2004).
26. Z. Yetgin, "Unsupervised change detection of satellite images using local gradual descent," *IEEE Trans. Geosci. Remote Sens.* **50**(5), 1919–1929 (2012).
27. A. Ghosh, N. S. Mishra, and S. Ghosh, "Fuzzy clustering algorithms for unsupervised change detection in remote sensing images," *Inf. Sci.* **181**(4), 699–715 (2011).

28. T. Celik, "Unsupervised change detection in satellite images using principal component analysis and k-means clustering," *IEEE Geosci. Remote Sens. Lett.* **6**(4), 772–776 (2009).

Yuqing Wu is mainly engaged in geographic information data analysis and mining, as well as intelligent interpretation of remote sensing images.

Biographies of the other authors are not available.